Semiclassical spatially dispersive intraband conductivity tensor and quantum capacitance of graphene

Giampiero Lovat,[1,*] George W. Hanson,[2,†] Rodolfo Araneo,[1,‡] and Paolo Burghignoli[3,§]

[1]*DIAEE, University of Rome "Sapienza," Via Eudossiana 18, 00184 Roma, Italy*

[2]*Department of Electrical Engineering, University of Wisconsin-Milwaukee, 3200 N. Cramer St., Milwaukee, Wisconsin 53211, USA*

[3]*D.I.E.T., University of Rome "Sapienza," Via Eudossiana 18, 00184 Roma, Italy*

(Received 4 January 2013; published 21 March 2013)

Analytical expressions are presented for the intraband conductivity tensor of graphene that includes spatial dispersion for arbitrarily wave-vector values and the presence of a nonzero Fermi energy. The conductivity tensor elements are derived from the semiclassical Boltzmann transport equation under both the relaxation-time approximation and the Bhatnagar-Gross-Krook model (which allows for an extra degree of freedom to enforce number conservation). The derived expressions are based on linear electron dispersion near the Dirac points, and extend previous results that assumed small wave-vector values; these are shown to be inadequate for the very slow waves expected on graphene nanoribbons. The new expressions are also compared to results obtained by numerical integration over the first Brillouin zone using the exact (tight-binding) electron dispersion relation. Very good agreement is found between the new analytical expressions and the exact numerical results. Furthermore, a comparison with the longitudinal random-phase conductivity is also made. It is shown analytically that these new expressions lead to the correct value of the quantum capacitance of a graphene sheet and that ignoring spatial dispersion leads to serious errors in the propagation properties of fundamental modes on graphene nanoribbons.

DOI: 10.1103/PhysRevB.87.115429 PACS number(s): 41.20.Jb, 73.22.Pr

I. INTRODUCTION

Graphene, which is a planar atomic layer of carbon atoms bonded in a hexagonal structure, is a very promising material in emerging nanoelectronic and nanoelectromagnetic applications and is attracting an enormous interest both theoretically and experimentally; the possible electromagnetic applications include screens, antennas, interconnects, polarizers, plasmonics, and cloaking.[1–11]

From an electronic point of view, graphene is a zero-band-gap semiconductor whose conductivity can be tuned either by doping or by electrostatic and/or magnetostatic bias through the electric-field and Hall effects.[12] From an electromagnetic point of view, graphene can be described as an infinitesimally thin medium characterized by a surface conductivity; based on a semiclassical description through the Boltzmann transport equation, a mathematical model for such a conductivity has been derived in the past, which also includes the important effects of electrostatic bias and doping.[13] Furthermore, it should be noted that under certain conditions spatial-dispersion effects may arise, which lead to a tensorial description of the graphene conductivity.[13]

Analytical expressions for the elements of the conductivity tensor have previously been obtained under the so-called low-q approximation (i.e., through a power series expansion for $q v_F \ll \omega$, where $q = |\mathbf{q}|$ is the amplitude of the spectral wave number, v_F is the Fermi velocity, and ω is the radian frequency of the electromagnetic field), so the model is expected to be valid for sufficiently fast waves. In fact, it has been shown that in these cases (e.g., for surface waves supported by isolated graphene sheets), for frequencies below the terahertz regime where interband transitions can be neglected, spatial dispersion effects can be ignored.[13] However, it has recently been shown that both simple two-dimensional graphene nanowaveguides and graphene nanoribbons (GNRs) can support extremely slow fundamental quasitransverse electromagnetic (TEM) modes in the low-frequency regime.[14] In such cases, spatial dispersion can become important and the low-q conductivity model is expected to be inaccurate.

In Ref. 13, the Boltzmann transport equation has been solved for the graphene conductivity tensor in the so-called relaxation-time approximation (RTA).[15] However, as is well known, the RTA approximation does not enforce charge conservation (see, e.g., Refs. 16 and 17, and references therein). If charge diffusion is included, as in the Bhatnagar-Gross-Krook (BGK) model,[18] a correction term is obtained (also known as the Mermin correction)[16] which can be important in deriving the quantum capacitance of a graphene sheet, similar to what has been shown for CNTs.[17]

In this paper, we derive the semiclassical, spatially dispersive intraband graphene conductivity tensor (the dominant contribution up to tens of THz, ignoring interband transitions) in the presence of an electric field, harmonic in space and time, given by $\mathbf{E}(\mathbf{r},t) = \mathbf{E}_0 e^{i(\mathbf{q}\cdot\mathbf{r}-\omega t)}$. We extend previous work in several ways. We first calculate the conductivity elements via numerical integration over the first Brillouin zone, based on the exact (tight-binding) electron dispersion relation. Next, based on the assumption of linear dispersion near the Dirac points, we derive approximate analytical expressions for the conductivity elements, valid at arbitrary wave vector. We compare the RTA and BGK results, and we show that in order to derive the correct quantum capacitance of a graphene sheet it is essential to include spatial dispersion effects in a Mermin-correction/BGK model. We also compare to the longitudinal quantum random-phase approximation (RPA) conductivity. Finally, we show that including spatial dispersion for arbitrary wave-vector values (including both nonlocality and the tensor character) in the graphene conductivity at low frequencies is important to obtain the correct dispersion behavior of the dominant modes on GNRs—in this case, neither the simple assumption of scalar

local conductivity, nor the low-q spatial dispersion model, is sufficient.

The present analysis is based on the Boltzmann transport equation, which becomes inapplicable when the spatial variation of the fields becomes comparable to the de Broglie wavelength of the particles (approximately, $q > 2k_F$, where k_F is the Fermi wave vector). Although this is not a practical restriction for our purposes, it may be for static-screening problems where $q > 2k_F$ may be of interest.[19,20]

II. SEMICLASSICAL GRAPHENE INTRABAND CONDUCTIVITY

As is well known, graphene is characterized by the energy function $\varepsilon(\mathbf{k})$, which reads

$$\varepsilon^{\pm}(\mathbf{k}) = \varepsilon^{\pm}(k_x,k_y) \simeq \pm\gamma_0 \frac{w(k_x,k_y)}{1 \mp s_0 w(k_x,k_y)}, \tag{1}$$

where

$$w(k_x,k_y) = \sqrt{1+4\cos\left(\frac{\sqrt{3}\,a}{2}k_x\right)\cos\left(\frac{a}{2}k_y\right)+4\cos^2\left(\frac{a}{2}k_y\right)}. \tag{2}$$

These expressions result from a nearest-neighbor tight-binding (NNTB) model, with possibly no electron-hole symmetry (in the case $s_0 \neq 0$).[21,22] The nearest-neighbor overlap energy γ_0 and the overlap integral s_0 can be used as fitting parameters to match first-principles computations or experimental data; commonly used values are $\gamma_0 = 3.033$ eV and $s_0 = 0.129$, respectively.[21] Finally, $a = \sqrt{3}\,b$ is the graphene lattice constant ($b = 0.142$ nm is the approximate length of the carbon-carbon bond in graphene), while the upper and lower signs in Eq. (1) correspond to the electrons in the conduction (π^*) and in the valence (π) bands, respectively. We can thus introduce the electron velocities $\mathbf{v}^+$ and $\mathbf{v}^-$ in the π^* and π bands, respectively, as

$$\mathbf{v}^{\pm} = \frac{1}{\hbar}\nabla_{\mathbf{k}}\varepsilon^{\pm}(\mathbf{k}). \tag{3}$$

The electron current density is

$$\begin{aligned}\mathbf{J} &= \mathbf{J}|_{\pi^*\text{ band}} + \mathbf{J}|_{\pi\text{ band}} = \mathbf{J}_e + \mathbf{J}_h \\ &= 2\frac{e}{(2\pi)^2}\iint_{BZ}\mathbf{v}^+(\mathbf{k})\,f_e(\mathbf{k})\,d^2\mathbf{k}\Big|_{\pi^*\text{ band}} \\ &\quad + 2\frac{(-e)}{(2\pi)^2}\iint_{BZ}\mathbf{v}^-(\mathbf{k})\,f_h(\mathbf{k})\,d^2\mathbf{k}\Big|_{\pi\text{ band}},\end{aligned} \tag{4}$$

where BZ indicates the first Brillouin zone, e is the electronic charge, while spin degeneracy is taken into account by the factor 2. The function $f_e = 1 - f_h$ represents the *nonequilibrium* distribution function for electrons.

Starting from the Boltzmann equation for electrons in the π^* and π bands together with the BGK model[17,18] (which allows an extra degree of freedom with respect to the usual relaxation-time approximation to enforce the current continuity equation), a perturbation approach leads to $f_e = f_e^{(0)} + f_e^{(1)}$ and $f_h = 1 - f_e = f_h^{(0)} + f_h^{(1)}$, where $|f_{e/h}^{(1)}| \ll |f_{e/h}^{(0)}|$, so that[17]

$$f_{e/h}^{(1)}(\mathbf{k}) = \frac{i h_{e/h}(\mathbf{k})\,\tau^{-1} - ie\frac{\partial f_e^{(0)}}{\partial\varepsilon}\mathbf{v}^{\pm}(\mathbf{k})\cdot\mathbf{E}}{\omega + i\tau^{-1} - \mathbf{v}^{\pm}(\mathbf{k})\cdot\mathbf{q}}, \tag{5}$$

where τ is a phenomenological electron relaxation time and

$$f_e^{(0)}(\varepsilon) = 1 - f_h^{(0)}(\varepsilon) = \frac{1}{1+e^{\frac{\varepsilon-\mu}{k_B T}}} \tag{6}$$

is the electron Fermi-Dirac distribution at equilibrium with a possibly nonzero chemical potential (Fermi level) μ, due either to doping or to an external electrostatic bias. Moreover, k_B is the Boltzmann constant, T is the temperature, and

$$h_{e/h}(\mathbf{k}) = \left.\frac{\partial f_{e/h}}{\partial n_{e/h}}\right|_0 \left(n_{e/h} - n_{e/h}^{(0)}\right), \tag{7}$$

where $n_{e/h}$ is the charge carrier density and $n_{e/h}^{(0)}$ is the charge carrier density at equilibrium, i.e.,

$$\begin{aligned} n_{e/h} &= \frac{2}{(2\pi)^2}\iint_{BZ} f_{e/h}(\mathbf{k})\,d^2\mathbf{k}, \\ n_{e/h}^{(0)} &= \frac{2}{(2\pi)^2}\iint_{BZ} f_{e/h}^{(0)}(\mathbf{k})\,d^2\mathbf{k}. \end{aligned} \tag{8}$$

Note that the term involving $h_{e/h}$ is absent in the RTA as in Ref. 17, so that the first term in Eq. (5) leads to diffusion current associated with the Mermin/BGK correction and the second term in Eq. (5) leads to drift current associated with the RTA method. Therefore, from Eqs. (4) and (5), we have

$$\begin{aligned}\mathbf{J} = \mathbf{J}_e + \mathbf{J}_h &= i\frac{e\tau^{-1}}{2\pi^2}\iint_{BZ}\frac{\mathbf{v}^+\,h_e(\mathbf{k})|_{\pi^*\text{band}}}{\omega + i\tau^{-1} - \mathbf{v}^+\cdot\mathbf{q}} \\ &\quad - \frac{\mathbf{v}^-\,h_h(\mathbf{k})|_{\pi\text{band}}}{\omega + i\tau^{-1} - \mathbf{v}^-\cdot\mathbf{q}}\,d^2\mathbf{k} \\ &\quad - i\frac{e^2}{2\pi^2}\iint_{BZ}\left.\frac{\partial f_e^{(0)}}{\partial\varepsilon}\right|_{\pi^*\text{ band}}\frac{\mathbf{v}^+\mathbf{v}^+\cdot\mathbf{E}}{\omega + i\tau^{-1} - \mathbf{v}^+\cdot\mathbf{q}} \\ &\quad + \left.\frac{\partial f_e^{(0)}}{\partial\varepsilon}\right|_{\pi\text{ band}}\frac{\mathbf{v}^-\mathbf{v}^-\cdot\mathbf{E}}{\omega + i\tau^{-1} - \mathbf{v}^-\cdot\mathbf{q}}\,d^2\mathbf{k},\end{aligned} \tag{9}$$

where

$$\begin{aligned}\mathbf{J}_e &= i\frac{e\tau^{-1}}{2\pi^2}\iint_{BZ}\frac{\mathbf{v}^+\,h_e(\mathbf{k})|_{\pi^*\text{band}}}{\omega + i\tau^{-1} - \mathbf{v}^+\cdot\mathbf{q}}\,d^2\mathbf{k} \\ &\quad - i\frac{e^2}{2\pi^2}\iint_{BZ}\left.\frac{\partial f_e^{(0)}}{\partial\varepsilon}\right|_{\pi^*\text{ band}}\frac{\mathbf{v}^+\mathbf{v}^+\cdot\mathbf{E}}{\omega + i\tau^{-1} - \mathbf{v}^+\cdot\mathbf{q}}\,d^2\mathbf{k} \\ &= \mathbf{J}_e^{\text{diff}} + \mathbf{J}_e^{\text{dr}}\end{aligned} \tag{10}$$

and

$$\begin{aligned}\mathbf{J}_h &= -i\frac{e\tau^{-1}}{2\pi^2}\iint_{BZ}\frac{\mathbf{v}^-\,h_h(\mathbf{k})|_{\pi\text{band}}}{\omega + i\tau^{-1} - \mathbf{v}^-\cdot\mathbf{q}}\,d^2\mathbf{k} \\ &\quad - i\frac{e^2}{2\pi^2}\iint_{BZ}\left.\frac{\partial f_e^{(0)}}{\partial\varepsilon}\right|_{\pi\text{ band}}\frac{\mathbf{v}^-\mathbf{v}^-\cdot\mathbf{E}}{\omega + i\tau^{-1} - \mathbf{v}^-\cdot\mathbf{q}}\,d^2\mathbf{k} \\ &= \mathbf{J}_h^{\text{diff}} + \mathbf{J}_h^{\text{dr}}.\end{aligned} \tag{11}$$

The first integrals on the RHS of Eqs. (10) and (11) define the diffusion currents $\mathbf{J}_{e/h}^{\text{diff}}$, while the second integrals define the drift currents $\mathbf{J}_{e/h}^{\text{dr}}$.

A. Drift currents and RTA conductivity

Let us consider first the drift currents $\mathbf{J}^{\rm dr}_{\rm e/h}$. Since

$$\frac{\partial f^{(0)}_{\rm e}}{\partial \varepsilon} = -\frac{1}{4k_{\rm B}T\cosh^2\left(\frac{\varepsilon-\mu}{2k_{\rm B}T}\right)}, \tag{12}$$

we have

$$\begin{aligned}\mathbf{J}^{\rm dr}_{\rm e/h} &= \frac{ie^2}{8k_{\rm B}T\pi^2}\iint_{\rm BZ}\frac{\mathbf{v}^{\pm}\mathbf{v}^{\pm}}{\cosh^2\left[\frac{\varepsilon^{\pm}(\mathbf{k})-\mu}{2k_{\rm B}T}\right](\omega+i\tau^{-1}-\mathbf{v}^{\pm}\cdot\mathbf{q})}\\ &\quad\times d^2\mathbf{k}\cdot\mathbf{E}_0e^{i\mathbf{q}\cdot\mathbf{r}}\\ &= \underline{\boldsymbol{\sigma}}^{\rm RTA}_{\rm e/h}\cdot\mathbf{E}_0e^{i\mathbf{q}\cdot\mathbf{r}},\end{aligned} \tag{13}$$

where, explicitly,

$$\underline{\boldsymbol{\sigma}}^{\rm RTA}_{\rm e/h} = \frac{ie^2}{8k_{\rm B}T\pi^2}\underline{\mathbf{A}}_{\rm ee/hh}(\mathbf{q}) \tag{14}$$

with

$$\underline{\mathbf{A}}_{\rm ee/hh}(\mathbf{q}) = \iint_{\rm BZ}\frac{\mathbf{v}^{\pm}\mathbf{v}^{\pm}}{\cosh^2\left[\frac{\varepsilon^{\pm}(\mathbf{k})-\mu}{2k_{\rm B}T}\right](\omega+i\tau^{-1}-\mathbf{v}^{\pm}\cdot\mathbf{q})}d^2\mathbf{k}. \tag{15}$$

Therefore we can write

$$\mathbf{J}_{\rm dr} = \mathbf{J}_{\rm e_{dr}} + \mathbf{J}_{\rm h_{dr}} = \underline{\boldsymbol{\sigma}}^{\rm RTA}\cdot\mathbf{E}_0e^{i\mathbf{q}\cdot\mathbf{r}}, \tag{16}$$

where

$$\underline{\boldsymbol{\sigma}}^{\rm RTA} = \underline{\boldsymbol{\sigma}}^{\rm RTA}_{\rm e} + \underline{\boldsymbol{\sigma}}^{\rm RTA}_{\rm h}. \tag{17}$$

This is the so-called RTA conductivity, obtained by neglecting diffusion currents (i.e., $h_{\rm e/h}=0$).[15]

B. Diffusion currents and the BGK conductivity

In order to evaluate the diffusion currents $\mathbf{J}^{\rm diff}_{\rm e/h}$, it should be noted that

$$\begin{aligned}&h_{\rm e/h}(\mathbf{k})|_{\pi^*/\pi\text{ band}}\\ &= \left.\frac{\partial f_{\rm e/h}}{\partial n_{\rm e/h}}\right|_0\left(n_{\rm e/h}-n^{(0)}_{\rm e/h}\right) = \frac{\partial f^{(0)}_{\rm e/h}}{\partial\mu}\left.\frac{\partial\mu}{\partial n_{\rm e/h}}\right|_0 n^{(1)}_{\rm e/h}e^{i\mathbf{q}\cdot\mathbf{r}}\\ &= \mp\frac{\partial f^{(0)}_{\rm e}}{\partial\varepsilon}\bigg|_{\varepsilon^{\pm}(\mathbf{k})}\left.\frac{\partial\mu}{\partial n_{\rm e/h}}\right|_0 n^{(1)}_{\rm e/h}e^{i\mathbf{q}\cdot\mathbf{r}}\\ &= \mp\frac{\partial f^{(0)}_{\rm e}}{\partial\varepsilon}\bigg|_{\varepsilon^{\pm}(\mathbf{k})}\left(\frac{\partial n^{(0)}_{\rm e/h}}{\partial\mu}\right)^{-1}n^{(1)}_{\rm e/h}e^{i\mathbf{q}\cdot\mathbf{r}}.\end{aligned} \tag{18}$$

Therefore, from Eq. (8), we obtain

$$\begin{aligned}\frac{\partial n^{(0)}_{\rm e/h}}{\partial\mu} &= \frac{1}{2\pi^2}\iint_{\rm BZ}\frac{\partial f^{(0)}_{\rm e/h}}{\partial\mu}d^2\mathbf{k}\\ &= \mp\frac{1}{2\pi^2}\iint_{\rm BZ}\frac{\partial f^{(0)}_{\rm e}}{\partial\varepsilon}\bigg|_{\varepsilon^{\pm}(\mathbf{k})}d^2\mathbf{k},\end{aligned} \tag{19}$$

so that

$$h_{\rm e/h}(\mathbf{k})\big|_{\pi^*/\pi\text{ band}} = \frac{2\pi^2}{F_{\rm e/h}\cosh^2\left[\frac{\varepsilon^{\pm}(\mathbf{k})-\mu}{2k_{\rm B}T}\right]}n^{(1)}_{\rm e/h}e^{i\mathbf{q}\cdot\mathbf{r}} \tag{20}$$

with

$$F_{\rm e/h} = \iint_{\rm BZ}\frac{1}{\cosh^2\left[\frac{\varepsilon^{\pm}(\mathbf{k})-\mu}{2k_{\rm B}T}\right]}d^2\mathbf{k}. \tag{21}$$

In this way, we have

$$\begin{aligned}\mathbf{J}^{\rm diff}_{\rm e/h} &= \pm\frac{ie\tau^{-1}}{2\pi^2}\iint_{\rm BZ}\frac{\mathbf{v}^{\pm}h_{\rm e/h}(\mathbf{k})|_{\pi^*/\pi\text{band}}}{\omega+i\tau^{-1}-\mathbf{v}^{\pm}\cdot\mathbf{q}}d^2\mathbf{k}\\ &= \mp\omega e\mathbf{d}_{\rm e/h}(\mathbf{q})\,n^{(1)}_{\rm e/h}e^{i\mathbf{q}\cdot\mathbf{r}},\end{aligned} \tag{22}$$

where

$$\begin{aligned}\mathbf{d}_{\rm e/h}(\mathbf{q}) &= -\frac{i}{\omega\tau F_{\rm e/h}}\\ &\quad\times\iint_{\rm BZ}\frac{\mathbf{v}^{\pm}}{\cosh^2\left[\frac{\varepsilon^{\pm}(\mathbf{k})-\mu}{2k_{\rm B}T}\right](\omega+i\tau^{-1}-\mathbf{v}^{\pm}\cdot\mathbf{q})}d^2\mathbf{k}.\end{aligned} \tag{23}$$

Now we enforce the continuity equation for the total electron or hole current $\nabla\cdot\mathbf{J}_{\rm e/h}-i\omega\rho_{\rm e/h}=0$. In the Fourier domain, taking into account that $\rho_{\rm e/h}=\pm en_{\rm e/h}$, we have

$$n^{(1)}_{\rm e/h} = \pm\frac{q_xJ_{e_x}+q_yJ_{e_y}}{\omega e} \tag{24}$$

so that

$$\mathbf{J}^{\rm diff}_{\rm e/h} = \mp\mathbf{d}_{\rm e/h}\left(q_xJ_{\rm e/h_x}+q_yJ_{\rm e/h_y}\right)e^{i\mathbf{q}\cdot\mathbf{r}}. \tag{25}$$

From Eqs. (9), (16), and (25), and suppressing the $e^{i\mathbf{q}\cdot\mathbf{r}}$ term, we have

$$\begin{aligned}\left(1+d_{\rm e_x}q_x\right)J_{\rm e_x}+d_{\rm e_x}q_yJ_{\rm e_y} &= \sigma^{\rm RTA}_{\rm e_{xx}}E_{0x}+\sigma^{\rm RTA}_{\rm e_{xy}}E_{0y},\\ d_{\rm e_y}q_xJ_{\rm e_x}+\left(1+d_{\rm e_y}q_y\right)J_{\rm e_y} &= \sigma^{\rm RTA}_{\rm e_{yx}}E_{0x}+\sigma^{\rm RTA}_{\rm e_{yy}}E_{0y},\end{aligned} \tag{26}$$

and

$$\begin{aligned}\left(1+d_{\rm h_x}q_x\right)J_{\rm h_x}+d_{\rm h_x}q_yJ_{\rm h_y} &= \sigma^{\rm RTA}_{\rm h_{xx}}E_{0x}+\sigma^{\rm RTA}_{\rm h_{xy}}E_{0y},\\ d_{\rm h_y}q_xJ_{\rm h_x}+\left(1+d_{\rm h_y}q_y\right)J_{\rm h_y} &= \sigma^{\rm RTA}_{\rm h_{yx}}E_{0x}+\sigma^{\rm RTA}_{\rm h_{yy}}E_{0y}.\end{aligned} \tag{27}$$

Equations (26) and (27) are two linear systems of two equations in two unknowns ($\{J_{\rm e_x},J_{\rm e_y}\}$ and $\{J_{\rm h_x},J_{\rm h_y}\}$), respectively. By solving them, we may finally express the graphene constitutive relation in the form

$$\mathbf{J} = \underline{\boldsymbol{\sigma}}^{\rm BGK}\cdot\mathbf{E}_0e^{i\mathbf{q}\cdot\mathbf{r}}, \tag{28}$$

where

$$\sigma^{\rm BGK}_{rs} = \sigma^{\rm e}_{rs}+\sigma^{\rm h}_{rs},\quad r,s=x,y, \tag{29}$$

and

$$\begin{aligned}\sigma^{\rm e/h}_{xx} &= \frac{\sigma^{\rm RTA}_{\rm e/h_{xx}}+q_y\left(\sigma^{\rm RTA}_{\rm e/h_{xx}}d_{\rm e/h_y}-\sigma^{\rm RTA}_{\rm e/h_{yx}}d_{\rm e/h_x}\right)}{1+\left(q_xd_{\rm e/h_x}+q_yd_{\rm e/h_y}\right)},\\ \sigma^{\rm e/h}_{xy} &= \frac{\sigma^{\rm RTA}_{\rm e/h_{xy}}+q_y\left(\sigma^{\rm RTA}_{\rm e/h_{xy}}d_{\rm e/h_y}-\sigma^{\rm RTA}_{\rm e/h_{yy}}d_{\rm e/h_x}\right)}{1+\left(q_xd_{\rm e/h_x}+q_yd_{\rm e/h_y}\right)},\\ \sigma^{\rm e/h}_{yx} &= \frac{\sigma^{\rm RTA}_{\rm e/h_{yx}}+q_x\left(\sigma^{\rm RTA}_{\rm e/h_{yx}}d_{\rm e/h_x}-\sigma^{\rm RTA}_{\rm e/h_{xx}}d_{\rm e/h_y}\right)}{1+\left(q_xd_{\rm e/h_x}+q_yd_{\rm e/h_y}\right)},\\ \sigma^{\rm e/h}_{yy} &= \frac{\sigma^{\rm RTA}_{\rm e/h_{yy}}+q_x\left(\sigma^{\rm RTA}_{\rm e/h_{yy}}d_{\rm e/h_x}-\sigma^{\rm RTA}_{\rm e/h_{xy}}d_{\rm e/h_y}\right)}{1+\left(q_xd_{\rm e/h_x}+q_yd_{\rm e/h_y}\right)}.\end{aligned} \tag{30}$$

The numerical evaluation of the integrals (15) and (23) over the 2D Brillouin zone cannot be performed analytically with the dispersion relation (1), but they can be performed numerically by discretizing the first Brillouin zone through nonoverlapping triangles and using Gaussian quadrature rules

and iterative techniques.[23] Results will be presented in a following section.

III. APPROXIMATE ANALYTICAL EVALUATION OF THE GRAPHENE CONDUCTIVITY: THE BGK AND RTA FORMS FOR ARBITRARY q VALUES

From the above formulation, it is possible to obtain approximate analytical expressions for the conductivity tensor by using the fact that the Dirac points (which coincide with the corners of the first Brillouin zone) give the most important contributions to the involved integrals.[24] Actually, this is strictly correct only when $\mu = 0$ eV; in fact, in general, the most important contributions come from the points where $\varepsilon = \mu$. When $\mu \neq 0$, we do not have isolated points at which $\varepsilon(\mathbf{k}) = \mu$ and by increasing μ the locus of such points gets further and further from the Dirac points $\mathbf{k}_{\mathrm{DP}}$. However, it can be shown numerically that the closed-form formulation derived below gives results with a relative error with respect to those obtained from Eq. (29) within 4%.

In the neighborhood of a Dirac point $\mathbf{k}_{\mathrm{DP}}$, we have a linear dispersion relation for the energy, i.e.,

$$\begin{aligned}\varepsilon^{\pm}(\mathbf{k}) &\simeq \pm\hbar v_{\mathrm{F}}\sqrt{(k_x - k_{\mathrm{F}x})^2 + (k_y - k_{\mathrm{F}y})^2} \\ &= \pm\hbar v_{\mathrm{F}}\,|\mathbf{k} - \mathbf{k}_{\mathrm{F}}|,\end{aligned} \tag{31}$$

where $v_{\mathrm{F}} = \sqrt{3}\,\gamma_0 a/(2\hbar) \simeq 10^8$ cm/s is the electron Fermi velocity. Starting from Eqs. (10) and (11) and following the procedure reported in the Appendix, we obtain the closed-form relation $\mathbf{J} = \underline{\boldsymbol{\sigma}}^{\mathrm{BGK}} \cdot \mathbf{E}_0$, where

$$\begin{aligned}\sigma_{xx}^{\mathrm{BGK}} &= \gamma\frac{I_{\phi_{xx}} + \gamma_{\mathrm{D}}\Delta q_y\left(I_{\phi_{xx}} q_y - I_{\phi_{yx}} q_x\right)}{D_\sigma}, \\ \sigma_{xy}^{\mathrm{BGK}} &= \gamma\frac{I_{\phi_{xy}} + \gamma_{\mathrm{D}}\Delta q_y\left(I_{\phi_{xy}} q_y - I_{\phi_{yy}} q_x\right)}{D_\sigma}, \\ \sigma_{yx}^{\mathrm{BGK}} &= \gamma\frac{I_{\phi_{yx}} + \gamma_{\mathrm{D}}\Delta q_x\left(I_{\phi_{yx}} q_x - I_{\phi_{xx}} q_y\right)}{D_\sigma}, \\ \sigma_{yy}^{\mathrm{BGK}} &= \gamma\frac{I_{\phi_{yy}} + \gamma_{\mathrm{D}}\Delta q_x\left(I_{\phi_{yy}} q_x - I_{\phi_{xy}} q_y\right)}{D_\sigma},\end{aligned} \tag{32}$$

with

$$\gamma = i\frac{e^2 k_{\mathrm{B}} T}{\pi^2\hbar^2}\,\ln\left\{2\left[1 + \cosh\left(\frac{\mu}{k_{\mathrm{B}}T}\right)\right]\right\}, \tag{33}$$

$$\gamma_{\mathrm{D}} = -i\frac{v_{\mathrm{F}}}{2\pi\omega\tau}, \tag{34}$$

and

$$D_\sigma = 1 + \gamma_{\mathrm{D}}\Delta q^2, \tag{35}$$

where the other symbols are defined in the Appendix. It should be noted that the presence of the term $\gamma_{\mathrm{D}}\Delta$ takes into account the diffusion process considered in the BGK formulation. Based on the above formulas, it can analytically be shown that the conductivity tensor is symmetric, i.e., $\sigma_{xy}^{\mathrm{BGK}} = \sigma_{yx}^{\mathrm{BGK}}$, in agreement with the Onsager reciprocity principle.[25]

It is interesting to note that the conductivity tensor has a diagonal form in a polar coordinate system. In fact, the matrix

$$\underline{\mathbf{M}} = \frac{1}{q}\begin{bmatrix} q_x & -q_y \\ q_y & q_x \end{bmatrix}, \tag{36}$$

which allows to change rectangular coordinates (x, y) to polar coordinates (ρ, ϕ), diagonalizes the conductivity tensor in Eq. (32), leading to the longitudinal and transverse conductivities, i.e.,

$$\underline{\boldsymbol{\sigma}}^{\mathrm{BGK}} = \begin{bmatrix} \sigma_\rho^{\mathrm{BGK}} & 0 \\ 0 & \sigma_\phi^{\mathrm{BGK}} \end{bmatrix}, \tag{37}$$

where

$$\sigma_\rho^{\mathrm{BGK}} = \frac{v_{\mathrm{F}}}{2\pi\gamma_{\mathrm{D}}(1-\chi) + v_{\mathrm{F}}\chi}\,\sigma_\phi^{\mathrm{BGK}}, \tag{38}$$

$$\sigma_\phi^{\mathrm{BGK}} = \gamma\frac{2\pi\alpha}{v_{\mathrm{F}}^2 q^2}(1-\chi), \tag{39}$$

and

$$\chi = \sqrt{1 - \frac{v_{\mathrm{F}}^2 q^2}{\alpha^2}}, \tag{40}$$

with $\alpha = \omega + i\tau^{-1}$. It should be noted that both $\sigma_\rho^{\mathrm{BGK}}$ and $\sigma_\phi^{\mathrm{BGK}}$ depend only on q. This implies that, within the limits of validity of the considered tensor conductivity model, a graphene sheet is *isotropic* in the xy plane, i.e., its constitutive relation relating the electric field and the surface current is invariant under arbitrary rotations of the sheet in that plane.[25]

It may also be noted that $\sigma_\phi^{\mathrm{BGK}}$ does not contain any diffusion terms. This may be expected, since the diffusion current arising in the Mermin-corrected BGK formulation derives from the enforcement of the conservation of electric charge, i.e., from the current continuity equation; the latter in the spectral domain reads $\mathbf{q}\cdot\mathbf{J} = qJ_\rho = \omega\rho$, hence it involves the radial current only. Therefore σ_ϕ obtained in the RTA formulation would give the same result as Eq. (39). In fact, in the RTA (i.e., neglecting the terms proportional to $\gamma_{\mathrm{D}}\Delta$), the conductivity $\underline{\boldsymbol{\sigma}}^{\mathrm{BGK}}$ reduces to

$$\underline{\boldsymbol{\sigma}}^{\mathrm{RTA}} = \gamma\underline{\mathbf{I}}_\phi. \tag{41}$$

In polar coordinates,

$$\sigma_\rho^{\mathrm{RTA}} = \frac{1}{\chi}\,\sigma_\phi^{\mathrm{RTA}}, \tag{42}$$

$$\sigma_\phi^{\mathrm{RTA}} = \sigma_\phi^{\mathrm{BGK}}. \tag{43}$$

It is interesting to note that for large q values (such that $|\alpha| \ll |v_{\mathrm{F}}q|$), the transverse conductivity becomes the dominant contribution since $|\sigma_\rho| \ll |\sigma_\phi|$.

IV. APPROXIMATE ANALYTICAL EVALUATION OF THE GRAPHENE CONDUCTIVITY: THE BGK AND RTA FORMS FOR LOW-q VALUES

By expanding the $\underline{\boldsymbol{\sigma}}^{\mathrm{BGK}}$ function in Eq. (32) in a Taylor series with respect to q_x and q_y we obtain the BGK low-q

model:

$$\begin{aligned}
\sigma_{xx}^{\mathrm{BGK}} &\simeq \gamma\frac{\pi}{\alpha}\left[1+\frac{v_{\mathrm{F}}^2}{4\alpha^2}\left(3+i\frac{2}{\omega\tau}\right)q_x^2+\frac{v_{\mathrm{F}}^2}{4\alpha^2}q_y^2\right],\\
\sigma_{xy}^{\mathrm{BGK}} &\simeq \gamma\frac{\pi}{\alpha}\left(\frac{v_{\mathrm{F}}^2}{2\alpha^2}\right)\left(1+i\frac{1}{\omega\tau}\right)q_xq_y,\\
\sigma_{yx}^{\mathrm{BGK}} &\simeq \gamma\frac{\pi}{\alpha}\left(\frac{v_{\mathrm{F}}^2}{2\alpha^2}\right)\left(1+i\frac{1}{\omega\tau}\right)q_xq_y,\\
\sigma_{yy}^{\mathrm{BGK}} &\simeq \gamma\frac{\pi}{\alpha}\left[1+\frac{v_{\mathrm{F}}^2}{4\alpha^2}q_x^2+\frac{v_{\mathrm{F}}^2}{4\alpha^2}\left(3+i\frac{2}{\omega\tau}\right)q_y^2\right].
\end{aligned}\tag{44}$$

By expanding the $\underline{\mathbf{I}}_\phi$ function (A18) in a Taylor series with respect to q_x and q_y, we obtain the RTA low-q model:

$$\begin{aligned}
\sigma_{xx}^{\mathrm{RTA}} &= \gamma I_{\phi_{xx}} \simeq \gamma\frac{\pi}{\alpha}\left(1+\frac{3v_{\mathrm{F}}^2}{4\alpha^2}q_x^2+\frac{v_{\mathrm{F}}^2}{4\alpha^2}q_y^2\right),\\
\sigma_{xy}^{\mathrm{RTA}} &= \gamma I_{\phi_{xy}} \simeq \gamma\frac{\pi}{\alpha}\left(\frac{v_{\mathrm{F}}^2}{2\alpha^2}\right)q_xq_y,\\
\sigma_{yx}^{\mathrm{RTA}} &= \gamma I_{\phi_{yx}} \simeq \gamma\frac{\pi}{\alpha}\left(\frac{v_{\mathrm{F}}^2}{2\alpha^2}\right)q_xq_y,\\
\sigma_{yy}^{\mathrm{RTA}} &= \gamma I_{\phi_{yy}} \simeq \gamma\frac{\pi}{\alpha}\left(1+\frac{v_{\mathrm{F}}^2}{4\alpha^2}q_x^2+\frac{3v_{\mathrm{F}}^2}{4\alpha^2}q_y^2\right).
\end{aligned}\tag{45}$$

As expected, expressions (45) are in a perfect agreement with the RTA conductivity derived in the limit of small q.[13]

In the absence of spatial dispersion (i.e., $\mathbf{q}=\mathbf{0}$), we have the scalar conductivity

$$\sigma = \gamma\frac{\pi}{\alpha},\tag{46}$$

which coincides with that derived in many other papers.[5,12,26,27]

As concerns the polar representation (37), for small q values, it is easy to show

$$\sigma_\rho^{\mathrm{BGK}} \simeq \gamma\frac{\pi}{\alpha}\left[1+\left(\frac{3}{4}+i\frac{1}{2\omega\tau}\right)\frac{v_{\mathrm{F}}^2}{\alpha^2}q^2\right],\tag{47}$$

$$\sigma_\phi^{\mathrm{BGK}} = \sigma_\phi^{\mathrm{RTA}} \simeq \gamma\frac{\pi}{\alpha}\left(1+\frac{v_{\mathrm{F}}^2}{4\alpha^2}q^2\right),\tag{48}$$

while

$$\sigma_\rho^{\mathrm{RTA}} \simeq \gamma\frac{\pi}{\alpha}\left[1+\frac{3v_{\mathrm{F}}^2}{4\alpha^2}q^2\right].\tag{49}$$

When $q=0$, we obtain

$$\sigma_\rho = \sigma_\phi = \gamma\frac{\pi}{\alpha},\tag{50}$$

which is again the scalar result obtained ignoring spatial dispersion.

Finally, the Lindhard/random phase approximation (RPA) leads to a longitudinal spatially dispersive conductivity,[28]

$$\sigma_\rho^{\mathrm{RPA}} = \gamma\frac{2\omega\pi}{2\omega\alpha - v_{\mathrm{F}}^2q^2}.\tag{51}$$

It should be noted also that the RPA conductivity is a low-q solution as well, since Eq. (51) is derived under the assumption $v_{\mathrm{F}}q \ll \omega$.[28] By normalizing q with respect to the free-space wave number $k_0=\omega/c$, the range of validity of the Lindhard/RPA model can also be expressed as $q/k_0 \ll c/v_{\mathrm{F}} \simeq 3\times10^2$.

V. QUANTUM CAPACITANCE OF A GRAPHENE SHEET

It is natural to define the graphene distributed impedance as $z = E_\rho/J_\rho = \sigma_\rho^{-1}$. In the low-$q$ approximation, the element σ_ρ can be written as

$$\sigma_\rho = \gamma\frac{\pi}{\alpha}(1+a_0q^2),\tag{52}$$

where the coefficient a_0 has different expressions in the BGK and RTA formulations,

$$a_0^{\mathrm{BGK}} = \left(\frac{3}{4}+i\frac{1}{2\omega\tau}\right)\frac{v_{\mathrm{F}}^2}{\alpha^2},\quad a_0^{\mathrm{RTA}} = \frac{3}{4}\frac{v_{\mathrm{F}}^2}{\alpha^2},\tag{53}$$

so that

$$\begin{aligned}
z = \frac{1}{\sigma_\rho} &= \frac{\alpha}{\gamma\pi(1+a_0q^2)}\\
&= \frac{1}{i\frac{e^2k_{\mathrm{B}}T}{\pi\hbar^2(\omega+i\tau^{-1})}\ln\left\{2\left[1+\cosh\left(\frac{\mu}{k_{\mathrm{B}}T}\right)\right]\right\}(1+a_0q^2)}\\
&\simeq \frac{\pi\hbar^2(1-i\omega\tau)}{e^2\tau k_{\mathrm{B}}T\ln\left\{2\left[1+\cosh\left(\frac{\mu}{k_{\mathrm{B}}T}\right)\right]\right\}}(1-a_0q^2)\\
&= R - i\omega L_{\mathrm{k}} + z_C,
\end{aligned}\tag{54}$$

where

$$R = \frac{\pi\hbar^2}{e^2\tau k_{\mathrm{B}}T\ln\left\{2\left[1+\cosh\left(\frac{\mu}{k_{\mathrm{B}}T}\right)\right]\right\}},\quad L_{\mathrm{k}} = \tau R.\tag{55}$$

The capacitance term is

$$\begin{aligned}
z_C &= -\frac{\pi\hbar^2(1-i\omega\tau)}{e^2\tau k_{\mathrm{B}}T\ln\left\{2\left[1+\cosh\left(\frac{\mu}{k_{\mathrm{B}}T}\right)\right]\right\}}a_0q^2\\
&= -\frac{1}{i\omega C_{\mathrm{q}}}\xi,
\end{aligned}\tag{56}$$

where

$$\xi = \frac{2i\omega(1-i\omega\tau)}{v_{\mathrm{F}}^2\tau}a_0q^2\tag{57}$$

and

$$C_{\mathrm{q}} = \frac{2e^2k_{\mathrm{B}}T\ln\left\{2\left[1+\cosh\left(\frac{\mu}{k_{\mathrm{B}}T}\right)\right]\right\}}{\pi\hbar^2v_{\mathrm{F}}^2}\tag{58}$$

agrees with the expression of the graphene quantum capacitance previously reported.[29,30]

First of all, it should be noted that the presence of quantum capacitance is a consequence of including spatial dispersion. Moreover, the parameter ξ is dramatically different in the BGK and the RTA models,

$$\begin{aligned}
\xi^{\mathrm{BGK}} &= -\left(\frac{3}{2}+i\frac{1}{\omega\tau}\right)\frac{i\omega\tau}{1-i\omega\tau}q^2,\\
\xi^{\mathrm{RTA}} &= -\frac{3}{2}\frac{i\omega\tau}{1-i\omega\tau}q^2.
\end{aligned}\tag{59}$$

The fundamental difference is that the coefficient ξ, which is frequency dependent, has a different limit for $\omega\to0$, so that

$$z^{\mathrm{BGK}} \to R - i\omega L_{\mathrm{k}} - \frac{q^2}{i\omega C_{\mathrm{q}}},\quad z^{\mathrm{RTA}} \to R - i\omega L_{\mathrm{k}}.\tag{60}$$

VI. NUMERICAL RESULTS

A. Graphene conductivity

In this section, a comparison among the different graphene conductivity models is presented for different radian frequencies ω, assuming in all cases $\tau = 0.5$ ps, $\mu = 0$ eV, and $T = 300$ K. The conductivity tensor will be represented in polar coordinates, showing results for σ_ρ and σ_ϕ as functions of the radial wave number q normalized with respect to the free-space wave number k_0.

For clarity, we summarize the different models considered. For the RTA formulations, there are three conductivity expressions; the one that is expected to be the most accurate over a wide range of q values is the result from numerical integration over the first BZ using the exact electron dispersion relation (1), leading to Eq. (17). The next most accurate formulation should be the full-q approximation where we assume linear dispersion (31) throughout the first BZ, leading to the analytical result (41). And, the least accurate (except for small q values) is expected to be the low-q analytical approximation (49) and (48). For the BGK result, which is expected to be more accurate than the RTA result, we again have three formulations that parallel the above-mentioned RTA ones; the result from numerical integration over the first BZ using the exact electron dispersion relation (1), leading to Eqs. (29) and (30), the full-q approximation where we assume linear dispersion (31) throughout the first BZ zone, leading to the analytical result (37), and the low-q analytical approximation (47) and (48). We also show the scalar, non-spatially-dispersive result (46) and also the Lindhard/RPA result (51).

In Fig. 1, the absolute values of σ_ρ and σ_ϕ are shown at $\omega/(2\pi) = 10$ GHz. The various formulations can be compared with the numerically exact reference result obtained by integrating over the Brillouin zone (thick blue line). For both components, the full-q RTA and BGK models are in excellent agreement with the reference results, respectively. However, the scalar, non-spatially-dispersive conductivity and both the low-q RTA and BGK models are accurate only in a low-q range, as expected; this range is however narrower for σ_ρ ($q < 1000k_0$) than for σ_ϕ ($q < 4000k_0$). Outside the low-q range, the numerically calculated RTA model for σ_ρ fails as well, thus showing the importance of the Mermin correction in modeling the longitudinal response of graphene.

It is interesting to observe that the longitudinal Lindhard/RPA formulation models very accurately σ_ρ, also well outside its expected range of validity $q/k_0 \ll 3 \times 10^2$.

In Fig. 2, results are shown for σ_ρ and σ_ϕ at the considerably higher frequency $\omega/(2\pi) = 1$ THz. While the full-q formulations remain accurate, the range of validity of the low-q formulations is reduced with respect to the previous case. The Lindhard/RPA model loses accuracy for $q/k_0 > 100$, as expected, but becomes again accurate at high wave numbers ($q/k_0 > 1000$). In fact, it can analytically be shown that in the asymptotic limit of large q/k_0 values the Lindhard/RPA scalar conductivity and the BGK full-q expression of σ_ρ converge to the same result.

For completeness, the real and imaginary parts of σ_ρ and σ_ϕ [computed using Eqs. (29) and (30)] are reported in Figs. 3(a) and 3(b), respectively, as functions of q/k_0 for different values of $\omega/(2\pi)$.

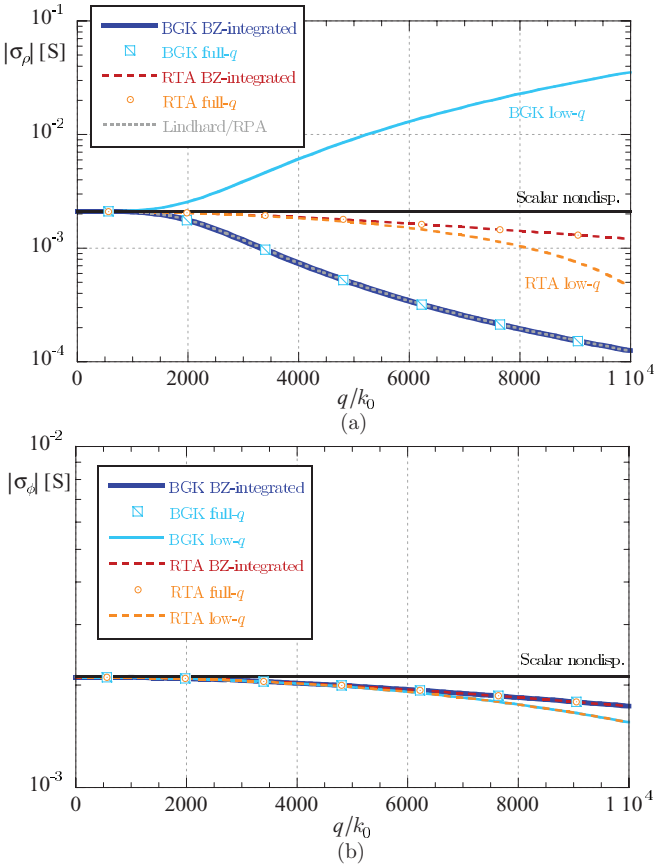

FIG. 1. (Color online) Absolute values of σ_ρ (a) and σ_ϕ (b) as functions of q/k_0 at $\omega/(2\pi) = 10$ GHz.

B. Graphene nanoribbon

In order to show the effects of spatial dispersion in graphene waveguiding structures, we study the dispersion properties of the fundamental mode supported by a graphene nanostrip line, i.e., a graphene nanoribbon (GNR) placed on a grounded dielectric substrate, as depicted in Fig. 4. In particular, a graphene strip of width w and of infinite length in the longitudinal y direction is assumed to be deposited over a SiO_2 substrate of thickness h, characterized by a relative permittivity ε_r and placed above a perfectly conducting (PEC) ground plane. Both the substrate and the ground plane are assumed to extend infinitely in the xy plane. The parameters of the structure are chosen as follows: $w = 100$ nm (two orders of magnitude larger than the graphene lattice constant a, so that electronic edge effects can be ignored), $h = 500$ nm, and $\varepsilon_r = 3.9$.

An integral equation for modal current density $\mathbf{J} = \mathbf{J}_0(x)\exp(-jq_y y)$ on the GNR is established by enforcing the constitutive relation (28) on the nanostrip and expressing the electric field in terms of $\mathbf{J}$ through the appropriate dyadic Green's functions for a grounded dielectric slab in the Fourier domain. Such an integral equation is then discretized with the method of moments, resulting in a linear homogeneous system whose coefficients depend on the modal wave number q_y; the latter can then be found through a numerical search for the zeros of the determinant of the system matrix in the complex

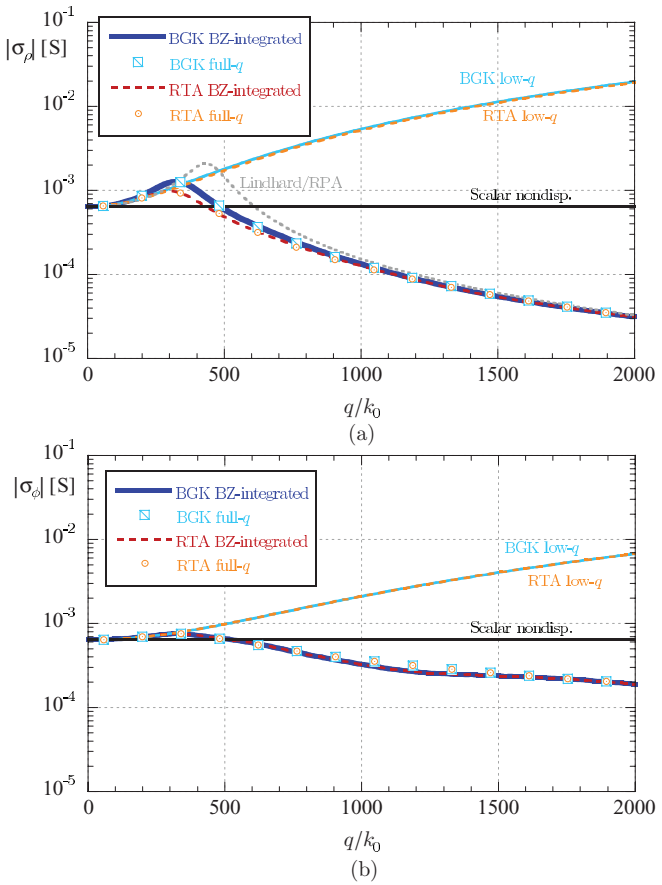

FIG. 2. (Color online) Absolute values of σ_ρ (a) and σ_ϕ (b) as functions of q/k_0 at $\omega/(2\pi) = 1$ THz.

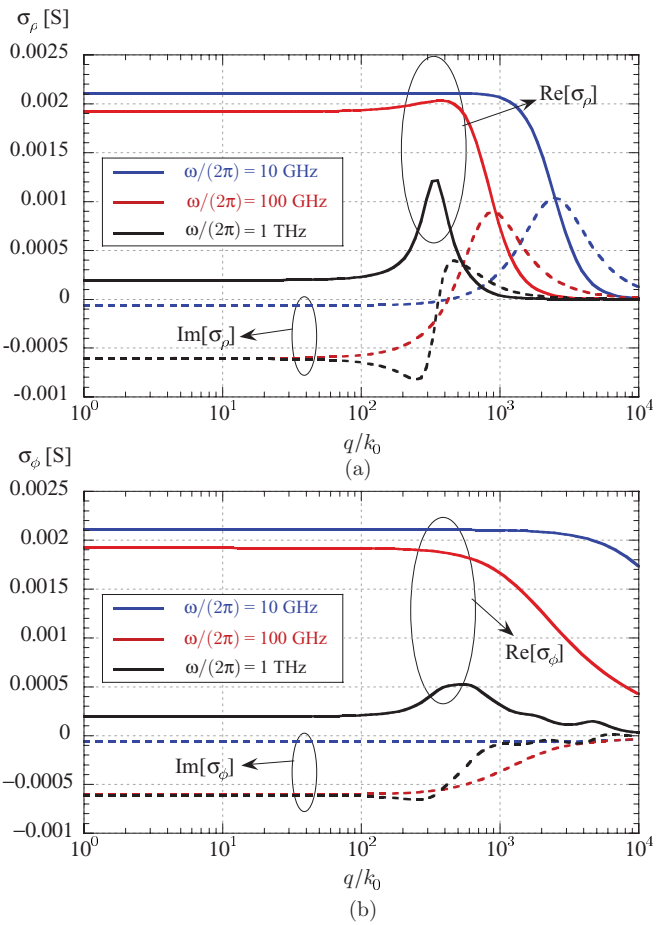

FIG. 3. (Color online) Real and imaginary parts of σ_ρ (a) and σ_ϕ (b) as functions of q/k_0 for different values of $\omega/(2\pi)$.

plane (more details can be found in Refs. 31 and 32). It is worth mentioning that in this formulation the coefficients of the linear system are expressed as inverse Fourier transforms, i.e., as integrals with respect to the transverse wave number q_x; when GNR with submicrometric widths are considered, the numerical evaluation of such coefficients may require the evaluation of the graphene conductivity tensor for high values of q_x/k_0, thus essentially requiring a representation of the conductivity tensor accurate in the high-q range. Since in this formulation the expression of the graphene conductivity in rectangular coordinates is required, for illustration purposes in Fig. 5 the real and imaginary parts of the elements σ_{xx}, σ_{xy}, and σ_{yy} of the graphene conductivity tensor are reported in the (q_x, q_y) plane at $\omega/(2\pi) = 100$ GHz.

In Fig. 6, dispersion and attenuation properties are illustrated for the considered nanostrip line in the frequency range from 1 GHz to 1 THz. In particular, on the bottom horizontal axis, the modal phase constant $\mathrm{Re}(q_y)$ is reported, normalized with respect to the free-space wave number k_0; on the top horizontal axis, the modal propagation length L_a is reported, normalized with respect to the modal guided wavelength λ_g, where $L_a/\lambda_g = \mathrm{Re}(q_y)/[2\pi\,\mathrm{Im}(q_y)]$. The nondispersive result is obtained using the scalar, q-independent result (46). As it can be seen, ignoring spatial dispersion leads to dramatic errors in the computation of the complex wave number q_y of the fundamental mode. In order to point out other effects of spatial dispersion, in Fig. 7, the amplitude of the y-component J_y of the modal current distribution on the nanostrip (normalized to its maximum value through the strip) is reported as a function of the normalized coordinate x/w at $\omega/(2\pi) = 100$ GHz (it is worth noting that the longitudinal component J_y is three orders of magnitude larger than the transverse component J_x). As can be seen, the almost constant behavior obtained ignoring spatial dispersion is very different from that obtained including the correct spatially dispersive behavior. Therefore the correct inclusion of spatial dispersion in the conductivity

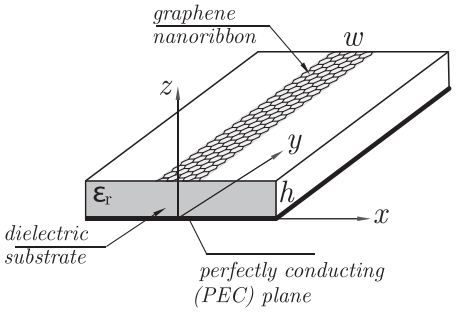

FIG. 4. Graphene nanoribbon over a grounded dielectric substrate.

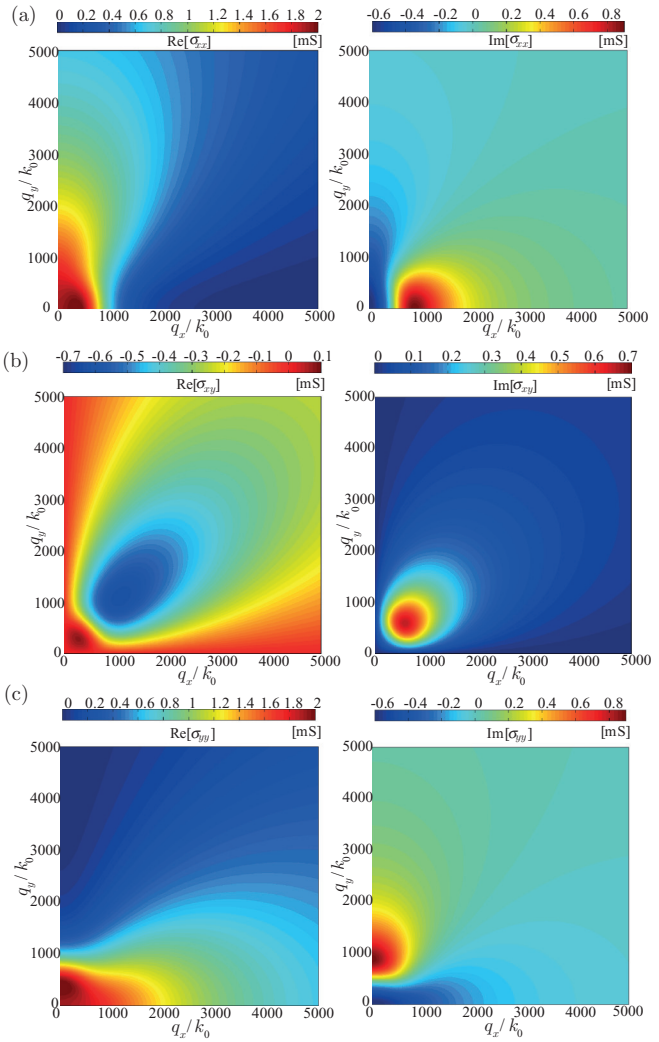

FIG. 5. (Color online) Real and imaginary parts of σ_{xx} (a), σ_{xy} (b), and σ_{yy} (c) as functions of q_x/k_0 and q_y/k_0 at $\omega/(2\pi) = 100$ GHz.

model of graphene is mandatory to derive reliable results for this particular problem.

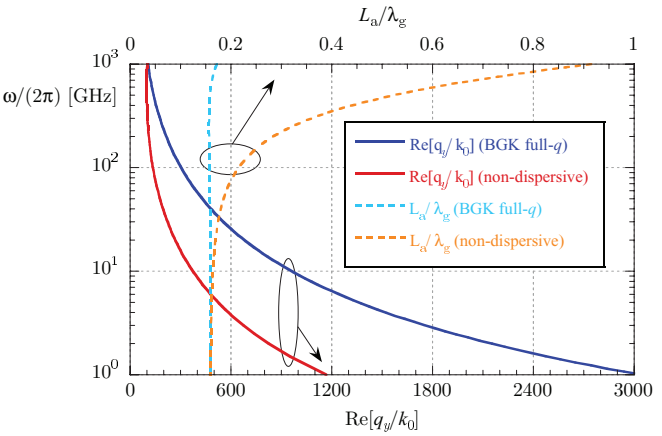

FIG. 6. (Color online) Normalized modal phase constant q_y/k_0 and normalized modal propagation length L_a/λ_g for a graphene nanostrip line with parameters $w = 100$ nm, $h = 500$ nm, and $\varepsilon_r = 3.9$.

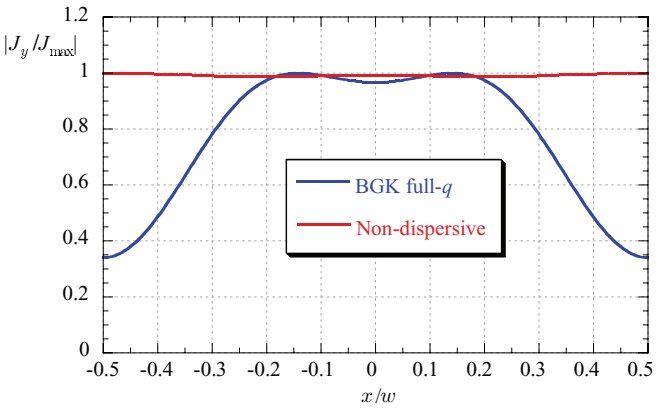

FIG. 7. (Color online) Normalized amplitude of the longitudinal component J_y of the modal current distribution as a function of the normalized abscissa x/w at $\omega/(2\pi) = 100$ GHz using the nondispersive and the BGK full-q model.

VII. CONCLUSION

This work presents analytical expressions for the semiclassical intraband conductivity tensor of graphene, which include spatial-dispersion effects for arbitrary wave-vector values (within the semiclassical Boltzmann-transport approach). Such expressions are derived in a rectangular coordinate system and are shown to give rise to a diagonal tensor in a polar coordinate system depending only on the radial wave number, thus clearly revealing the isotropic nature of graphene despite the tensor representation. Moreover, the elements of the graphene conductivity tensor, derived under the linear electron dispersion approximation, are compared with results obtained by numerical integration over the first Brillouin zone using the exact (tight-binding) electron dispersion relation showing an excellent agreement for Fermi energies up to 1 eV. These new expressions, obtained under the Bhatnagar-Gross-Krook model (which allows for enforcing charge conservation and thus modeling diffusion currents), are also shown to lead to the correct expression for the quantum capacitance of a graphene sheet. Finally, as a case study, it is shown that ignoring spatial dispersion in the conductivity model of graphene results in dramatic errors in the computation of the propagation properties of graphene nanoribbons.

APPENDIX

We report in this Appendix the derivation of the expressions (32). By assuming the validity of Eq. (31) over the entire Brillouin zone, we have

$$\mathbf{v}^{\pm}(\mathbf{k}) = \pm v_F \frac{\mathbf{k} - \mathbf{k}_F}{|\mathbf{k} - \mathbf{k}_F|}. \tag{A1}$$

Upon defining a coordinate system centered at $\mathbf{k}_F$ (where $\varepsilon = 0$), we may write

$$\mathbf{v}^{\pm}(\mathbf{k}) = \pm v_F \frac{\mathbf{k}}{|\mathbf{k}|}. \tag{A2}$$

By using a polar coordinate system for $\mathbf{k}$ (i.e., $k_x = k_\rho \cos\phi_k$ and $k_y = k_\rho \sin\phi_k$), from Eqs. (10) and (11), we obtain

$$\mathbf{J}_{\mathrm{e/h}} = \pm i \frac{e\tau^{-1}}{2\pi^2} \iint_{\mathrm{BZ}} \frac{h_{\mathrm{e/h}}(\varepsilon^{\pm})\mathbf{v}^{\pm}(k_\rho,\phi_k)}{\omega + i\tau^{-1} - \mathbf{v}^{\pm}(k_\rho,\phi_k)\cdot\mathbf{q}}\, k_\rho\, dk_\rho\, d\phi_k - i\frac{e^2}{2\pi^2} \iint_{\mathrm{BZ}} \left.\frac{\partial f_{\mathrm{e}}^{(0)}}{\partial\varepsilon}\right|_{\varepsilon^{\pm}} \frac{\mathbf{v}^{\pm}(k_\rho,\phi_k)\mathbf{v}^{\pm}(k_\rho,\phi_k)\cdot\mathbf{E}}{\omega + i\tau^{-1} - \mathbf{v}^{\pm}(k_\rho,\phi_k)\cdot\mathbf{q}} \times k_\rho\, dk_\rho\, d\phi_k. \tag{A3}$$

We can now make the change of variable $\varepsilon = \hbar v_{\mathrm{F}} k_\rho$. From Eq. (A3), we thus obtain for the electron current $\mathbf{J}_{\mathrm{e}}$ (conduction band, with positive energies) and the hole current $\mathbf{J}_{\mathrm{h}}$ (valence band, with negative energies),

$$\mathbf{J}_{\mathrm{e/h}} = \pm i \frac{e\tau^{-1}}{2\pi^2\hbar^2 v_{\mathrm{F}}^2} \times 2\int_0^{2\pi}\int_0^{\pm\infty} \frac{h_{\mathrm{e/h}}(\varepsilon)\,\mathbf{v}^{\pm}(\varepsilon,\phi_k)}{\omega + i\tau^{-1} - \mathbf{v}^{\pm}(\varepsilon,\phi_k)\cdot\mathbf{q}}\, \varepsilon\, d\varepsilon\, d\phi_k - i\frac{e^2}{2\pi^2\hbar^2 v_{\mathrm{F}}^2} 2\int_0^{2\pi}\int_0^{\pm\infty} \left.\frac{\partial f_{\mathrm{e}}^{(0)}}{\partial\varepsilon}\right|_{\varepsilon} \times \frac{\mathbf{v}^{\pm}(\varepsilon,\phi_k)\,\mathbf{v}^{\pm}(\varepsilon,\phi_k)\cdot\mathbf{E}}{\omega + i\tau^{-1} - \mathbf{v}^{\pm}(\varepsilon,\phi_k)\cdot\mathbf{q}}\, \varepsilon\, d\varepsilon\, d\phi_k, \tag{A4}$$

which can also be written as

$$\mathbf{J}_{\mathrm{e/h}} = \pm i \frac{e\tau^{-1}}{2\pi^2\hbar^2 v_{\mathrm{F}}^2} \times 2\int_0^{2\pi}\int_0^{+\infty} \frac{h_{\mathrm{e/h}}(\pm\varepsilon)\,\mathbf{v}^{\pm}(\pm\varepsilon,\phi_k)}{\omega + i\tau^{-1} - \mathbf{v}^{\pm}(\pm\varepsilon,\phi_k)\cdot\mathbf{q}}\, \varepsilon\, d\varepsilon\, d\phi_k - i\frac{e^2}{2\pi^2\hbar^2 v_{\mathrm{F}}^2} 2\int_0^{2\pi}\int_0^{+\infty} \left.\frac{\partial f_{\mathrm{e}}^{(0)}}{\partial\varepsilon}\right|_{\pm\varepsilon} \times \frac{\mathbf{v}^{\pm}(\pm\varepsilon,\phi_k)\,\mathbf{v}^{\pm}(\pm\varepsilon,\phi_k)\cdot\mathbf{E}}{\omega + i\tau^{-1} - \mathbf{v}^{\pm}(\pm\varepsilon,\phi_k)\cdot\mathbf{q}}\, \varepsilon\, d\varepsilon\, d\phi_k. \tag{A5}$$

It should then be noted that $\mathbf{v}^{-}(-\varepsilon,\phi_k) = \mathbf{v}^{+}(\varepsilon,\phi_k)$ and therefore

$$\mathbf{J}_{\mathrm{e/h}} = \pm i \frac{e\tau^{-1}}{2\pi^2\hbar^2 v_{\mathrm{F}}^2} \times 2\int_0^{2\pi}\int_0^{+\infty} \frac{h_{\mathrm{e/h}}(\pm\varepsilon)\,\mathbf{v}^{+}(\varepsilon,\phi_k)}{\omega + i\tau^{-1} - \mathbf{v}^{+}(\varepsilon,\phi_k)\cdot\mathbf{q}}\, \varepsilon\, d\varepsilon\, d\phi_k - i\frac{e^2}{2\pi^2\hbar^2 v_{\mathrm{F}}^2} 2\int_0^{2\pi}\int_0^{+\infty} \left.\frac{\partial f_{\mathrm{e}}^{(0)}}{\partial\varepsilon}\right|_{\pm\varepsilon} \times \frac{\mathbf{v}^{+}(\varepsilon,\phi_k)\,\mathbf{v}^{+}(\varepsilon,\phi_k)\cdot\mathbf{E}}{\omega + i\tau^{-1} - \mathbf{v}^{+}(\varepsilon,\phi_k)\cdot\mathbf{q}}\, \varepsilon\, d\varepsilon\, d\phi_k. \tag{A6}$$

From Eq. (A6), we thus have

$$\mathbf{J} = \mathbf{J}_{\mathrm{e}} + \mathbf{J}_{\mathrm{h}} = i\frac{e\tau^{-1}}{\pi^2\hbar^2 v_{\mathrm{F}}^2} \times \int_0^{2\pi}\int_0^{+\infty} \frac{[h_{\mathrm{e}}(\varepsilon) - h_{\mathrm{h}}(-\varepsilon)]\,\mathbf{v}^{+}(\varepsilon)}{\omega + i\tau^{-1} - \mathbf{v}^{+}(\varepsilon,\phi_k)\cdot\mathbf{q}}\, \varepsilon\, d\varepsilon\, d\phi_k - i\frac{e^2}{2\pi^2\hbar^2 v_{\mathrm{F}}^2} 2\int_0^{2\pi}\int_0^{+\infty} \left[\left.\frac{\partial f_{\mathrm{e}}^{(0)}}{\partial\varepsilon}\right|_{\varepsilon} + \left.\frac{\partial f_{\mathrm{e}}^{(0)}}{\partial\varepsilon}\right|_{-\varepsilon}\right] \times \frac{\mathbf{v}^{+}(\varepsilon,\phi_k)\,\mathbf{v}^{+}(\varepsilon,\phi_k)\cdot\mathbf{E}}{\omega + i\tau^{-1} - \mathbf{v}^{+}(\varepsilon,\phi_k)\cdot\mathbf{q}}\, \varepsilon\, d\varepsilon\, d\phi_k. \tag{A7}$$

By replacing

$$\mathbf{v}^{+}(\varepsilon,\phi_k) = v_{\mathrm{F}}(\mathbf{u}_x\cos\phi_k + \mathbf{u}_y\sin\phi_k) = v_{\mathrm{F}}\mathbf{u}_k, \tag{A8}$$

we finally have

$$\mathbf{J} = i\frac{e\tau^{-1}}{\pi^2\hbar^2 v_{\mathrm{F}}} \int_0^{2\pi}\int_0^{+\infty} \frac{[h_{\mathrm{e}}(\varepsilon) - h_{\mathrm{h}}(-\varepsilon)]\,\mathbf{u}_k}{\omega + i\tau^{-1} - v_{\mathrm{F}}\mathbf{u}_k\cdot\mathbf{q}}\, \varepsilon\, d\varepsilon\, d\phi_k - i\frac{e^2}{2\pi^2\hbar^2} 2\int_0^{2\pi}\int_0^{+\infty} \left[\left.\frac{\partial f_{\mathrm{e}}^{(0)}}{\partial\varepsilon}\right|_{\varepsilon} + \left.\frac{\partial f_{\mathrm{e}}^{(0)}}{\partial\varepsilon}\right|_{-\varepsilon}\right] \times \frac{\mathbf{u}_k\mathbf{u}_k\cdot\mathbf{E}}{\omega + i\tau^{-1} - v_{\mathrm{F}}\mathbf{u}_k\cdot\mathbf{q}}\, \varepsilon\, d\varepsilon\, d\phi_k. \tag{A9}$$

It can be observed that the double integrals in Eq. (A9) are actually products of single integrals, i.e.,

$$\mathbf{J} = \frac{ie}{\pi^2\hbar^2 v_{\mathrm{F}}} \left\{ \tau^{-1}\int_0^{+\infty} \varepsilon\,[h_{\mathrm{e}}(\varepsilon) - h_{\mathrm{h}}(-\varepsilon)]\, d\varepsilon \times \int_0^{2\pi} \frac{\mathbf{u}_k}{\omega + i\tau^{-1} - v_{\mathrm{F}}\mathbf{u}_k\cdot\mathbf{q}}\, d\phi_k - ev_{\mathrm{F}}\int_0^{+\infty} \varepsilon \left[\left.\frac{\partial f_{\mathrm{e}}^{(0)}}{\partial\varepsilon}\right|_{\varepsilon} + \left.\frac{\partial f_{\mathrm{e}}^{(0)}}{\partial\varepsilon}\right|_{-\varepsilon}\right] d\varepsilon \times \int_0^{2\pi} \frac{\mathbf{u}_k\mathbf{u}_k}{\omega + i\tau^{-1} - v_{\mathrm{F}}\mathbf{u}_k\cdot\mathbf{q}}\, d\phi_k\cdot\mathbf{E} \right\}, \tag{A10}$$

which can be expressed as

$$\mathbf{J} = \frac{ie}{\pi^2\hbar^2 v_{\mathrm{F}}\tau}\, D_\varepsilon \mathbf{D}_\phi(\mathbf{q}) - \frac{ie^2}{\pi^2\hbar^2}\, I_\varepsilon \underline{\mathbf{I}}_\phi(\mathbf{q})\cdot\mathbf{E}_0 e^{i\mathbf{q}\cdot\mathbf{r}}, \tag{A11}$$

where

$$\mathbf{D}_\phi(\mathbf{q}) = \int_0^{2\pi} \frac{\mathbf{u}_k}{\omega + i\tau^{-1} - v_{\mathrm{F}}\mathbf{u}_k\cdot\mathbf{q}}\, d\phi_k, \tag{A12}$$

$$\underline{\mathbf{I}}_\phi(\mathbf{q}) = \int_0^{2\pi} \frac{\mathbf{u}_k\mathbf{u}_k}{\omega + i\tau^{-1} - v_{\mathrm{F}}\mathbf{u}_k\cdot\mathbf{q}}\, d\phi_k, \tag{A13}$$

$$I_\varepsilon = \int_0^{+\infty} \varepsilon \left[\left.\frac{\partial f_{\mathrm{e}}^{(0)}}{\partial\varepsilon}\right|_{\varepsilon} + \left.\frac{\partial f_{\mathrm{e}}^{(0)}}{\partial\varepsilon}\right|_{-\varepsilon}\right] d\varepsilon. \tag{A14}$$

These integrals can now be calculated exactly in closed form. In particular, we have

$$D_{\phi_x}(q_x,q_y) = \Delta(q_x,q_y)\, q_x, \quad D_{\phi_y}(q_x,q_y) = \Delta(q_x,q_y)\, q_y, \tag{A15}$$

where

$$\Delta(q_x,q_y) = -\frac{2\pi}{v_F q^2}\left(1 - \frac{\alpha}{\sqrt{\alpha^2 - v_F^2 q^2}}\right), \tag{A16}$$

$$R(q_x,q_y) = \frac{\alpha + v_F q_x}{\sqrt{\alpha^2 - v_F^2 q^2}}, \tag{A17}$$

and $\alpha = \omega + i\tau^{-1}$, while $q^2 = q_x^2 + q_y^2$. We also have

$$\begin{aligned} I_{\phi_{xx}}(q_x,q_y) &= 2\pi \frac{v_F^2 q_y^2 q^2 R - \alpha v_F q_x p^2 - \alpha^2 p^2 (1-R)}{v_F^2 (\alpha + v_F q_x) q^4}, \\ I_{\phi_{xy}}(q_x,q_y) &= I_{\phi_{yx}}(q_x,q_y) = -2\pi q_x q_y \\ &\quad \times \frac{v_F^2 q^2 R + 2\alpha v_F q_x + 2\alpha^2 (1-R)}{v_F^2 (\alpha + v_F q_x) q^4}, \\ I_{\phi_{yy}}(q_x,q_y) &= 2\pi \frac{v_F^2 q_x^2 q^2 R + \alpha v_F q_x p^2 + \alpha^2 p^2 (1-R)}{v_F^2 (\alpha + v_F q_x) q^4}, \end{aligned} \tag{A18}$$

where $p^2 = q_x^2 - q_y^2$.

It is also simple to show that

$$I_\varepsilon = -k_B T \ln\left\{2\left[1 + \cosh\left(\frac{\mu}{k_B T}\right)\right]\right\}. \tag{A19}$$

In order to evaluate the D_ε function, we need to calculate first the terms h_e and h_h. We have

$$\begin{aligned} h_e(\varepsilon) &= \left.\frac{\partial f_e}{\partial n_e}\right|_0 \left(n_e - n_e^{(0)}\right) = \left.\frac{\partial f_e^{(0)}}{\partial \mu}\,\frac{\partial \mu}{\partial n_e}\right|_0 n_e^{(1)} e^{i\mathbf{q}\cdot\mathbf{r}} \\ &= -\left.\frac{\partial f_e^{(0)}}{\partial \varepsilon}\,\frac{\partial \mu}{\partial n_e}\right|_0 n_e^{(1)} e^{i\mathbf{q}\cdot\mathbf{r}} \end{aligned} \tag{A20}$$

and

$$\begin{aligned} h_h(-\varepsilon) &= \left.\frac{\partial f_h(-\varepsilon)}{\partial n_e}\right|_0 \left(n_h - n_h^{(0)}\right) \\ &= -\left.\frac{\partial f_e^{(0)}(-\varepsilon)}{\partial \varepsilon}\,\frac{\partial \mu}{\partial n_h}\right|_0 n_h^{(1)} e^{i\mathbf{q}\cdot\mathbf{r}}. \end{aligned} \tag{A21}$$

Moreover, from

$$\begin{aligned} n_e^{(0)} &= \frac{2}{(2\pi)^2}\iint_{BZ} f_e^{(0)}(\varepsilon)\, d^2\mathbf{k} \\ &= \frac{2}{\pi\hbar^2 v_F^2}\int_0^{+\infty} f_e^{(0)}(\varepsilon)\,\varepsilon\, d\varepsilon, \\ n_h^{(0)} &= \frac{2}{(2\pi)^2}\iint_{BZ} f_h^{(0)}(\varepsilon)\, d^2\mathbf{k} \\ &= \frac{2}{\pi\hbar^2 v_F^2}\int_0^{+\infty} f_e^{(0)}(\varepsilon + 2\mu)\varepsilon\, d\varepsilon, \end{aligned} \tag{A22}$$

we obtain

$$\frac{\partial n_{e/h}^{(0)}}{\partial \mu} = \pm\frac{2k_B T}{\pi\hbar^2 v_F^2}\ln\left(1 + e^{\pm\frac{\mu}{k_B T}}\right), \tag{A23}$$

so that

$$D_\varepsilon = \int_0^{+\infty} \varepsilon[h_e(\varepsilon) - h_h(-\varepsilon)]\, d\varepsilon = \frac{\pi\hbar^2 v_F^2}{2}\left(n_e^{(1)} - n_h^{(1)}\right)e^{i\mathbf{q}\cdot\mathbf{r}}. \tag{A24}$$

Finally, from the continuity equation

$$\nabla_{\mathbf{r}}\cdot\mathbf{J} = i\omega\rho = i\omega e\left(n_e^{(1)} - n_h^{(1)}\right), \tag{A25}$$

we have

$$n_e^{(1)} - n_h^{(1)} = \frac{q_x J_x + q_y J_y}{\omega e}. \tag{A26}$$

By suppressing the $e^{i\mathbf{q}\cdot\mathbf{r}}$ term, from Eqs. (A11), (A24), and (A26), using Eq. (A15) and defining

$$\gamma_D = -i\frac{v_F}{2\pi\omega\tau}, \tag{A27}$$

we obtain

$$\begin{aligned} &J_x\left(1 + \gamma_D \Delta q_x^2\right) + J_y(\gamma_D \Delta q_x q_y) \\ &\quad = -\frac{ie^2}{\pi^2\hbar^2} I_\varepsilon \left(I_{\phi_{xx}} E_{0x} + I_{\phi_{xy}} E_{0y}\right), \\ &J_x(\gamma_D \Delta q_x q_y) + J_y\left(1 + \gamma_D \Delta q_y^2\right) \\ &\quad = -\frac{ie^2}{\pi^2\hbar^2} I_\varepsilon \left(I_{\phi_{yx}} E_{0x} + I_{\phi_{yy}} E_{0y}\right), \end{aligned} \tag{A28}$$

which is a linear system of two equations in two unknowns J_x and J_y. By representing the solution of Eq. (A28) as $\mathbf{J} = \underline{\boldsymbol{\sigma}}\cdot\mathbf{E}_0$, we finally obtain the tensor elements in Eq. (32).

*giampiero.lovat@uniroma1.it
†george@uwm.edu
‡rodolfo.araneo@uniroma1.it
§burghignoli@die.uniroma1.it

[1] C. Xu, H. Li, and K. Banerjee, IEEE Trans. Electron Devices **56**, 1567 (2009).
[2] A. Vakil and N. Engheta, Science **332**, 1291 (2011).
[3] P.-Y. Chen and A. Alù, ACS Nano **5**, 5855 (2011).
[4] G. Lovat, IEEE Trans. Electromagn. Compat. **54**, 101 (2012).
[5] A. Y. Nikitin, F. Guinea, F. J. García-Vidal, and L. Martín-Moreno, Phys. Rev. B **84**, 161407 (2011).
[6] J. Christensen, A. Manjavacas, S. Thongrattanasiri, F. H. L. Koppens, and F. J. Garca de Abajo, ACS Nano **6**, 431 (2012).
[7] P. Liu, W. Cai, L. Wang, X. Zhang, and J. Xu, Appl. Phys. Lett. **100**, 153111 (2012).
[8] A. Y. Nikitin, F. Guinea, F. J. García-Vidal, and L. Martín-Moreno, Phys. Rev. B **85**, 081405 (2012).
[9] P. A. Huidobro, A. Y. Nikitin, C. González-Ballestero, L. Martín-Moreno, and F. J. García-Vidal, Phys. Rev. B **85**, 155438 (2012).
[10] A. Vakil and N. Engheta, Phys. Rev. B **85**, 075434 (2012).
[11] F. Hipolito, A. J. Chaves, R. M. Ribeiro, M. I. Vasilevskiy, V. M. Pereira, and N. M. R. Peres, Phys. Rev. B **86**, 115430 (2012).

[12]V. P. Gusynin, S. G. Sharapov, and J. P. Carbotte, J. Phys.: Condens. Matter **19**, 026222 (2007).
[13]G. W. Hanson, IEEE Trans. Antennas Propag. **56**, 747 (2008).
[14]G. Lovat, P. Burghignoli, and R. Araneo, IEEE Trans. Electromagn. Compat. **55**, 101 (2013).
[15]N. W. Ashcroft and N. D. Mermin, *Solid State Physics* (Brooks-Cole, Belmont, CA, 1976).
[16]N. D. Mermin, Phys. Rev. B **1**, 2362 (1970).
[17]G. W. Hanson, IEEE Trans. Microw. Theory Tech. **59**, 9 (2011).
[18]P. L. Bhatnagar, E. P. Gross, and M. Krook, Phys. Rev. **94**, 511 (1954).
[19]B. Wunsch, T. Stauber, F. Sols, and F. Guinea, New J. Phys. **8**, 318 (2006).
[20]E. H. Hwang and S. Das Sarma, Phys. Rev. B **75**, 205418 (2007).
[21]R. Saito, G. Dresselhaus, and M. S. Dresselhaus, *Physical Properties of Carbon Nanotubes* (Imperial College Press, London, UK, 1998).
[22]H.-S. P. Wong and D. Akinwande, *Carbon Nanotube and Graphene Device Physics* (Cambridge University Press, Cambridge, UK, 2011).
[23]D. A. Dunavant, Intern. J. Num. Meth. Engin. **21**, 1129 (1985).
[24]P. R. Wallace, Phys. Rev. **71**, 622 (1947).
[25]L. D. Landau and E. M. Lifshitz, *Electrodynamics of Continuous Media* (Pergamon, New York, 1984).
[26]L. A. Falkovsky, Physics-Uspekhi **51**, 887 (2008).
[27]G. W. Hanson, J. Appl. Phys. **103**, 064302 (2008).
[28]F. Rana, IEEE Trans. Nanotechnology **7**, 91 (2008).
[29]T. Fang, A. Konar, H. Xing, and D. Jena, Appl. Phys. Lett. **91**, 092109 (2007).
[30]J. Xia, F. Chen, J. Li, and N. Tao, Nat. Nanotechnology **4**, 505 (2009).
[31]R. Araneo, G. Lovat, and P. Burghignoli, in *Proceedings 16th IEEE Workshop on Signal and Power Integrity, SPI* (IEEE, Piscataway, NJ, 2012), pp. 75–78.
[32]R. Araneo, G. Lovat, and P. Burghignoli, in *Antennas and Propagation Society International Symposium (APSURSI), 2012 IEEE* (IEEE, Piscataway, NJ, 2012), pp. 1–2.